A Switching Active Sensing Strategy to Maintain Observability for Vision-Based Formation Control

Gian Luca Mariottini, Simone Martini, Magnus B. Egerstedt

***Abstract*— Vision-based control of a robot formation is challenging because the on-board sensor (camera) only provides the view-angle to the other moving robots, but not the distance that must be estimated. In order to guarantee a consistent estimate of the distance by knowing the control inputs and the sensor outputs in a given interval, the nonlinear multi-robot system must preserve its observability. Recent theoretical studies on leader-follower robot formation exploit the interesting influence that the control actions have on observability. Based on these results, in this paper we present a switching active control strategy for formation control. Our control strategy is active in the sense that, while asymptotically achieving the formation control tasks, it also guarantees the system observability in those cases in which all the robots tend to move along non-observable paths. As a result, both estimation and formation performances are improved. Extensive simulation results show the effectiveness of the proposed design.**

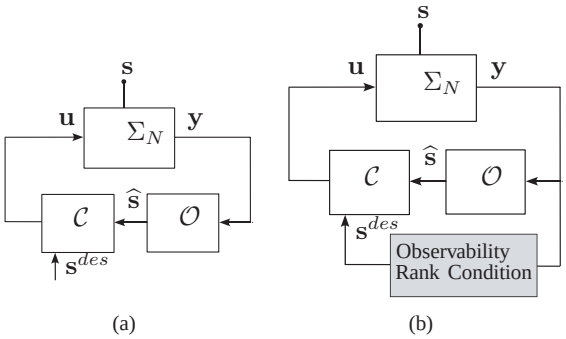

Fig. 1. (a) - *Traditional control scheme*: Sensed outputs $\mathbf{y}$ are used by the observer $\mathcal{O}$ to produce an estimate $\widehat{\mathbf{s}}$ of the robot formation state $\mathbf{s}$. The control law $\mathcal{C}$ uses $\widehat{\mathbf{s}}$ to achieve the desired formation goals. (b) - *Our switching active scheme* An analytical study of the observability (gray block) allows us to design a switching control law $\mathbf{u}$ that guarantees both the formation stability and the system observability.

I. Introduction

The proliferation of robotics devices and the growing number of their potential applications, recently lead to an increase of interest towards multiple-robot applications such as consensus, rendezvous, sensor coverage and simultaneous localization and mapping [1], [2].

Among these, *formation control* stimulated a great deal of research [3] due to its wide range of applicability. In particular, *leader-follower* formation control consists in controlling followers' relative distance and orientation with respect to an independently moving leader [4].

A challenging way to address this navigation problem is to use exclusively on-board passive vision sensors, like omnidirectional cameras which guarantee a 360° field-of-view. Visual sensors are particularly appealing due to their low cost compared to the rich information they provide when compared to other traditional robotic sensors (e.g. sonars, scanners). Other approaches have shown the vision-based control and localization for the cases of static landmarks [6], using motion segmentation techniques based on optical-flow [7] or with known camera calibration parameters [8]. However, we will henceforth assume that each robot is equipped with one uncalibrated panoramic camera which *only* provides the view-angle to other moving robots: in this case the formation control problem is challenging because of the unknown distance between the robots.

G.L. Mariottini is with Department of Computer Science and Engineering, University of Minnesota, Minneapolis, MN 55455, USA. M.B. Egerstedt is with the Department of Electrical and Computer Engineering, Georgia Institute of Technology, Atlanta, GA, 30332 USA. S. Martini is with the Dept. of Electrical Engineering, University of Pisa, Pisa, ITALY.
Corresponding author: gianluca@cs.umn.edu

In this respect, the formation control problem with vision sensors can be solved only if a *localization problem* has been first solved. Localization is basically an estimation problem in which the first issue to be addressed is the study of observability. A system is said to be observable when it is possible to reconstruct the initial state by knowing, in a given interval, both the control inputs and the measured outputs [9]. For a system to preserve the observability means that the sensor measurements will be "rich enough", thus implying that the error in the localization will be bounded.

In Fig. 1(a) we can observe a classic block diagram for the control of a system Σ (e.g. a multi-robot formation): an observer $\mathcal{O}$ uses the camera measurements $\mathbf{y}$ to provide an estimate $\hat{\mathbf{s}}$ of the system state $\mathbf{s}$. In the leader-follower scenario, the formation state consists of the relative distance, view-angle and heading between the i-th follower and the leader. The estimated state $\hat{\mathbf{s}}$ and the desired robot formation shape $\mathbf{s}^{des}$ are then used by the control law $\mathcal{C}$ to compute the steering inputs $\mathbf{u}$ needed to maintain the formation.

In the case of robotic platforms with on-board vision sensors, we are dealing with a nonlinear system and then only tools from differential nonlinear systems theory must be used to prove the possibility to reconstruct the state [10]. Based on [11], Mariottini *et al.* [12] presented a new *observability rank condition* valid for general nonlinear systems and based on the rank of the Extended Output Jacobian (EOJ) matrix. This new observability condition allows to recognize in real-time and directly from the sensor domain (image pixels) which are the robot controls that kill or preserve the system observability. An example of a odd situation is when the

robots reach *and* maintain straight formation trajectories: in this case the localization fails because the sensor outputs (view-angles) do not change due to the zero relative motion between the robots. As an effect, the process and the measurement noises can slowly accumulate in time and make the robots deviate from the nominal formation.

The innovative approach we present in this work makes use of a well-known property of nonlinear systems: differently from linear systems, the observability of a nonlinear system depends also on the inputs $\mathbf{u}$. This is particularly appealing because suggests that the design of $\mathbf{u}$ can affect (and hopefully improve) the performances of the observer and consequently those of the overall robot formation. Based on this property and as an innovative contribution, we present a control strategy that uses the determinant of the EOJ matrix to switch between two control laws: the first one, used when the system is observable, guarantees exponentially convergence to zero of the formation state tracking error; the second one, that starts when the observability rank condition is not verified, can be considered as an *active control law* because introduces some variations in the desired formation $\mathbf{s}^{des}$ to both guarantee the asymptotic formation tracking and the recovery of observability. See Fig. 1(b) for its block diagram. The proposed active control law has a closed-form expression that allows the study of stability. In this way our control follows a different direction from other "active-vision" strategies based on numerical optimization methods, whose gap is related with the impossibility to provide an analytical study for the asymptotic stability of the closed-loop system.

The paper is structured as follows: in Sect. II we introduce the leader-follower sensing and communication assumptions, together with the kinematic modelling. In Sect. III we present the Observability Rank Condition and use it to show the non-observable robot trajectories. The switching control strategy and the active control law are presented in Sect. IV, together with the stability analysis. Simulation results are presented in Sect. V., while concluding remarks are in Sect. VI.

II. The leader-follower sensing, communication and kinematic model

Let us consider the leader-follower setup in Fig. 2. Without losing in generality and for the sake of simplicity, hereafter we will consider only the case with one follower. The extension to multiple followers is straightforward [12].

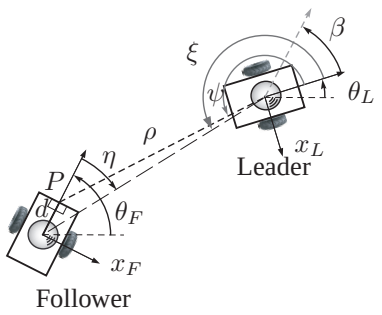

Fig. 2. Leader-follower setup in polar coordinates.

Each robot is equipped only with an omnidirectional camera [13]: the one on the leader measures the view-angles ξ and ψ given respectively by the observation of the follower's centroid and of the colored marker P placed at a known distance d (Fig. 2). Analogously, the camera on the follower can measure the view-angle η to the centroid of the leader. The angle η is then transmitted by the follower to the leader, thus allowing the calculation of the heading $\beta = -\xi + \eta + \pi$. To simplify the discussion, we will henceforth refer *only* to β, implicitly assuming the transmission of η.

To summarize, the *measurement vector* $\mathbf{y}$ on the leader is defined as

$$\mathbf{y} \triangleq [\psi \ \ \beta]^T. \tag{1}$$

The detection of the robot centroid and of the marker P is achieved using color blob extraction or active contour tracking [14].

The whole system can be modeled in polar coordinates with the state vector $\mathbf{s} \triangleq [\rho \ \psi \ \beta]^T$, where ρ is the distance from the center of the leader to the marker P. As mentioned in the Introduction, the leader uses the camera measurements $\mathbf{y}$ in (1) to provide a state estimate $\widehat{\mathbf{s}}$. The state $\widehat{\mathbf{s}}$ is then used to compute a control input $[u_F \ \ \omega_F]$ to be sent to each follower, in order to allow them to maintain a desired distance and orientation to the leader $\mathbf{s}_r = [\rho^{des} \ \psi^{des}]^T$.

The leader-follower system is described by the following model

Proposition 1 (Leader – follower kinematic model [12]): With reference to Fig. 2, the leader – follower kinematic model can be written as follows

$$\dot{\mathbf{s}} = \mathbf{G}(\mathbf{s})\,\mathbf{u}, \tag{2}$$

where $\mathbf{u} \triangleq [v_F \ \omega_F \ v_L \ \omega_L]^T$ and

$$\mathbf{G}(\mathbf{s}) = \begin{bmatrix} \cos\gamma & d\sin\gamma & -\cos\psi & 0 \\ \frac{-\sin\gamma}{\rho} & \frac{d\cos\gamma}{\rho} & \frac{\sin\psi}{\rho} & -1 \\ 0 & -1 & 0 & 1 \end{bmatrix} \tag{3}$$

where $\gamma \triangleq \beta + \psi$. ■

The kinematic model in the case of q followers can be obtained by simply extending (2).

Finally note that simple geometric considerations from Fig. 2, together with the knowledge of d, ψ and ξ, could have been used to analytically compute the distance ρ. However, since this is possible only when $\psi \neq \xi$ (i.e. non distant robots), we then adopted an EKF to avoid this problem, as detailed in Sect. V.

III. Observability of nonlinear systems

In this section we present the results on *observability* for generic nonlinear systems and apply them to the leader-follower system in (2).

A generic system Σ is of the form

$$\Sigma: \begin{cases} \dot{\mathbf{s}}(t) = \mathbf{f}(\mathbf{s}(t), \mathbf{u}(t)) \ , \quad \mathbf{s}(0) \equiv \mathbf{s}_0 \\ \mathbf{y}(t) = \mathbf{h}(\mathbf{s}(t)) = [h_1 \ h_2 \ ... \ h_m]^T \end{cases} \tag{4}$$

where $\mathbf{s}(t) \in I\!R^n$ is the state, $\mathbf{y}(t) \in I\!R^m$ are the sensors measurements and $\mathbf{u} \in I\!R^p$ is the input. As mentioned in the Introduction, and differently from linear systems, global or complete observability can not be usually expected for (4) and the notion of *local weak observability* at a point $\mathbf{s}_0$ has been introduced in [11].

A sufficient observability rank condition recently proposed in [12], states that (4) is locally weak observable at $\mathbf{s}_0$ if there exist an open set of $\mathbf{s}_0$ for which the Extended Output Jacobian matrix with rows

$$\mathbf{J} = \{dh_i^{(j-1)}(\mathbf{s}) \,|\, i = 1, ..., m \,;\, j = 1, ..., n\} \qquad (5)$$

is full rank. The superscript j refers to the order of time differentiation of the functions $h_i(\mathbf{s})$.

A. Vision-based observability of leader-follower

The above observability rank condition can be applied to the leader-follower setup of Prop. 1 with visual measurements as in (1) so to obtain the following observability condition

$$\det(\mathbf{J}) = \frac{1}{\rho}\left[\dot{\psi} + \omega_L\right] \neq 0. \qquad (6)$$

The above equation has an intuitive geometrical interpretation, as shown in Fig. 3: a leader $\langle L \rangle$ and two followers $\langle F_1 \rangle$, $\langle F_2 \rangle$ are here considered at two different time instants, $t = 0$ and $t = 1$. All the robots move with the same translational velocity and zero angular velocity ($\omega_L = 0$). After one step we note that $\psi_2(1) \neq \psi_2(0)$ (and thus $\dot{\psi}_2 \neq 0$) due to an initial heading different between $\langle L \rangle$ and $\langle F_2 \rangle$. Then, from (6), it turns out that the state $\mathbf{s}_2$ is observable. This is intuitively correct, since the visual information varies in time and it is then expected to improve the localizability. Analogously, *curvilinear trajectories* are expected to have a favourable effect on observability, since a change of the output signal (1) occurs there.

Remark 1 (Unobservable trajectories): In order to study unobservable trajectories, we would like to use the observability rank test as a necessary condition, while (6) is only sufficient. However, as pointed out in [11]-(Th. 3.11), the observability condition is necessary when the observability matrix is full rank everywhere except possibly within a subset of the domain of $\mathbf{s}$. Hence, if $\mathbf{J}$ is not of rank 3 for all values of $\mathbf{s}$, then the system is *not* locally weakly observable. From Fig.. 3 we can observe that the system made of $\langle L \rangle$ and $\langle F_1 \rangle$ is not observable, since $\dot{\psi}_1 = 0$. More in general,

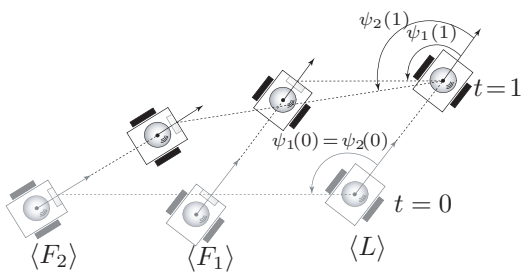

Fig. 3. Geometrical interpretation of the EOJ singularity.

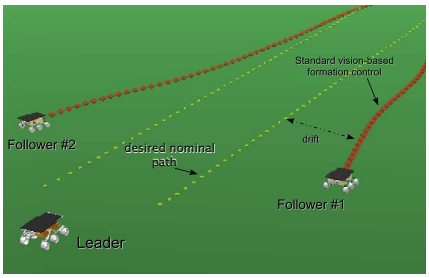

(a)

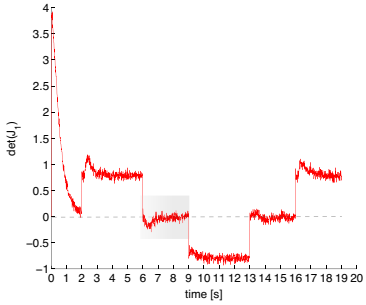

(b)

Fig. 4. Unobservable trajectories. (a) On rectilinear trajectories the visual information is not changing sensibly so as to improve the robot localization. This results in a drift of the robot trajectories with respect to the nominal (desired) ones. (b) The highlighted region indicates the time instants $t = [6, 9]$ sec. in which $\det(\mathbf{J})$ drops down to zero that also corresponds to the trajectory drift.

along rectilinear tracts $\dot{\mathbf{y}} = \ddot{\mathbf{y}} = \mathbf{0}$, thus implying that the system is not observable since $\text{rank}(\mathbf{J}) < 3$. In this situation, every kind of process noise (e.g. wheels slippage or unmodeled dynamics) is never corrected by the sensor data which is not informative along straight paths. To remark this phenomena, in Fig. 4(a) we show a snapshot from the simulation results, showing a leader and two followers along rectilinear trajectories (EKF is used here as the observer): while they are expected to move along straight nominal paths, their actual trajectories exhibit large drifts with respect to the desired trajectory. Also, exactly in correspondence of these drifts ($t = [6, 9]$ sec.) the value of $\det(\mathbf{J})$ drops down to zero in Fig. 4(b), thus revealing itself as an index of non-observability.

Remark 2: It is paramount to note that the observability condition (6) can be used to detect the observability in real-time. The leader needs only to compute $\dot{\psi}$ and to know ω_L.

IV. Vision-based Active Formation Control

In what follows we first review a *standard* input-state feedback formation control law used in [4], [12]. This control exponentially stabilizes to zero the formation tracking error (distance and angle)along all the trajectory. However, as shown in Fig.4(a), along rectilinear tracts the formation observability will not be preserved. In Prop. 2 we then introduce the main contribution of this paper, i.e. an *active control strategy* which guarantees both the asymptotic (but not exponential) convergence to zero of the formation tracking error along rectilinear tracts, as well as the system

observability. We finally present the switching strategy to switch from the standard to the active control in the case in which the observability condition (6) is not satisfied.

A. Standard leader-follower formation control

The leader-follower kinematics in (2) can be written as

$$\begin{cases} \dot{\mathbf{s}}_r = \mathbf{H}(\mathbf{s})\mathbf{u}_F + \mathbf{G}(\mathbf{s})\mathbf{u}_L \\ \dot{\beta} = \omega_L - \omega_F \end{cases} \tag{7}$$

where $\mathbf{s}_r \triangleq [\rho \;\; \psi]^T$ and

$$\mathbf{H}(\mathbf{s}) = \begin{bmatrix} \cos\gamma & d\sin\gamma \\ \frac{-\sin\gamma}{\rho} & \frac{d\cos\gamma}{\rho} \end{bmatrix}, \quad \mathbf{G}(\mathbf{s}) = \begin{bmatrix} -\cos\psi & 0 \\ \frac{\sin\psi}{\rho} & -1 \end{bmatrix}. \tag{8}$$

The following control law stabilizes the formation towards a certain desired state $\mathbf{s}_r^{des} = [\rho^{des} \;\; \psi^{des}]^T$ [15]:

$$\mathbf{u}_F = \mathbf{H}(\hat{\mathbf{s}})^{-1}(\mathbf{p} - \mathbf{G}(\hat{\mathbf{s}})\mathbf{u}_L), \tag{9}$$

with $\mathbf{p} \triangleq -\mathbf{K}\big(\widehat{\mathbf{s}}_r - \mathbf{s}_r^{\text{des}}\big) + \dot{\mathbf{s}}_r^{\text{des}}$ and where $\mathbf{K} = diag\{k_1, k_2\}$ with $k_1, k_2 > 0$. Equation (9) acts in (7) as a feedback linearizing control, so that the closed loop formation error dynamics

$$\dot{\mathbf{s}}_r = \mathbf{s}_r^{des} - \mathbf{K}(\mathbf{s}_r - \mathbf{s}_r^{des}), \quad \dot{\beta} = \omega_L - \omega_F \tag{10}$$

become exponentially convergent to zero [4].

B. The Active Formation Control Strategy

Proposition 2 (Active control law): Let $\widehat{\mathbf{s}}$ be an estimate of $\mathbf{s} = [\rho \; \psi \; \beta]^T$ as provided by the observer $\mathcal{O}$ and let also $\widehat{\mathbf{s}}_r = [\widehat{\rho} \;\; \widehat{\psi}]^T$. Then the control law

$$\widetilde{\mathbf{u}}_F = \mathbf{H}(\hat{\mathbf{s}})^{-1}(\widetilde{\mathbf{p}} - \mathbf{G}(\hat{\mathbf{s}})\mathbf{u}_L), \tag{11}$$

with

$$\widetilde{\mathbf{p}} \triangleq -\mathbf{K}(\widehat{\mathbf{s}}_r - \widetilde{\mathbf{s}}_r^{des}) + \dot{\widetilde{\mathbf{s}}}_r^{des}, \tag{12}$$

where

$$\widetilde{\mathbf{s}}_r^{des} \triangleq [\rho^{des}, \;\; \psi^{des} + \varepsilon_\psi]^T, \tag{13}$$

guarantees *both* the vision-based observability *and* the asymptotic stability of the formation tracking error $\mathbf{e} \triangleq \mathbf{s} - \mathbf{s}^{des}$ for any bounded $c(t) \neq 0 \;\forall t$ and for a choice of the function ε_ψ satisfying at the following differential constraint:

$$\dot{\varepsilon}_\psi + k_2\varepsilon_\psi + \Big(\omega_L - k_2(\psi - \psi^{des}) + \dot{\psi}^{des} - c(t)\Big) = 0, \tag{14}$$

that is true for this choice of ε_ψ

$$\varepsilon_\psi = -e^{-k_2 t}\int_0^t \Big(\omega_L - k_2(\psi - \psi_c^{des}) + \dot{\psi}^{des} - c(\tau)\Big)e^{k_2\tau}d\tau. \tag{15}$$

Proof: Using (11)-(12) in (7), the dynamics of the reduced state state $\mathbf{s}_r$ can be written as

$$\begin{aligned} \dot{\mathbf{s}}_r = \;& - \;\; \mathbf{H}(\mathbf{s})\mathbf{H}^{-1}(\widehat{\mathbf{s}})[\mathbf{K}(\widehat{\mathbf{s}}_r - \widetilde{\mathbf{s}}_r^{\text{des}}) - \dot{\widetilde{\mathbf{s}}}_r^{\text{des}}] + \\ & + \;\; [\mathbf{G}(\mathbf{s}) - \mathbf{H}(\mathbf{s})\mathbf{H}^{-1}(\widehat{\mathbf{s}})\mathbf{G}(\widehat{\mathbf{s}})]\mathbf{u}_L. \end{aligned} \tag{16}$$

Note that, using (8), (16) can be written as:

$$\dot{\mathbf{s}}_r = -\begin{bmatrix} k_1 & 0 \\ 0 & k_2\frac{\widehat{\rho}}{\rho} \end{bmatrix}(\widehat{\mathbf{s}}_r - \widetilde{\mathbf{s}}_r^{des}) + \begin{bmatrix} 1 & 0 \\ 0 & \frac{\widehat{\rho}}{\rho} \end{bmatrix}\dot{\widetilde{\mathbf{s}}}_r^{des} + \begin{bmatrix} 0 \\ \Big(\frac{\widehat{\rho}}{\rho} - 1\Big)\omega_L \end{bmatrix} \tag{17}$$

Substituting (13), the above equation becomes

$$\dot{\rho} = -k_1(\widehat{\rho} - \rho^{des}) + \dot{\rho}^{des} \tag{18}$$

$$\dot{\psi} = -k_2\frac{\widehat{\rho}}{\rho}(\psi - \psi^{des} - \varepsilon_\psi) + \frac{\widehat{\rho}}{\rho}\Big(\dot{\psi}^{des} + \dot{\varepsilon}_\psi\Big) + \Big(\frac{\widehat{\rho}}{\rho} - 1\Big)\omega_L. \tag{19}$$

For a given $c(t) \neq 0$, the observability condition in (6) can be used in (19) to obtain the following

$$\widehat{\rho} = \rho\,\underbrace{\frac{c(t)}{-k_2(\psi - \psi^{des}) + \dot{\psi}^{des} + \omega_L + k_2\varepsilon_\psi + \dot{\varepsilon}_\psi}}_{\alpha(t)}. \tag{20}$$

Using (20) into (18), a linear differential equation for the distance tracking error $e_\rho \triangleq \rho - \rho^{des}$ is obtained

$$\dot{\rho} = -k_1\left(\rho\frac{c(t)}{\alpha(t)} - \rho^{des}\right) + \dot{\rho}^{des}.$$

Imposing at this point the exponential stability of e_ρ, corresponds in constraining $\alpha(t) = c(t)$, i.e., from (20),

$$c(t) = -k_2(\psi - \psi^{des}) + \dot{\psi}^{des} + \omega_L + k_2\varepsilon_\psi + \dot{\varepsilon}_\psi \tag{21}$$

which gives the differential equation in (14).

The stability of $e_\psi = \psi - \psi^{des}$ can be studied using (21) to retrieve:

$$\dot{\psi} - \dot{\psi}^{des} = -k_2 e_\psi + \underbrace{(k_2\varepsilon_\psi + \dot{\varepsilon}_\psi)}_{p(t)}. \tag{22}$$

From (14), the perturbation $p(t) = -\omega_L + k_2 e_\psi - \dot{\psi}^{des} + c(t)$ is bounded, since ω_L, $c(t)$ and $\dot{\psi}^{des}$ are bounded also. The boundedness of $p(t)$ implies that $\psi - \psi^{des}$ is asymptotically stable. Finally, the stability of the internal dynamics β can be proved analogously as in [4]. ■

C. Switching strategy

We have just presented two control strategies, the one in (9) and the active one in (11). They only differ for the desired value given to the angle ψ^{des} that, in the active control strategy, is augmented by ε_ψ. The switching strategy block diagram is shown in Fig. 5: the standard control law (9) is used from the beginning and when the observability

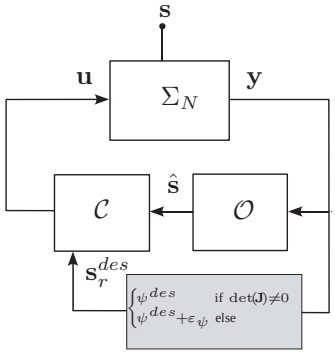

Fig. 5. Block diagram for the switching strategy. When the system becomes non-observable, i.e. (6) is not verified, the active strategy guarantees both the observability and the asymptotic tracking error stability.

condition (6) drops down to zero, then the active strategy in (11) is used.

In this way, when the robots are moving along observable paths then the exponential formation is guaranteed. Also, when they move along non-observable trajectories, then the active control guarantees the asymptotic convergence of the formation and the maintenance of the observability.

V. Simulation Results

This section presents extensive simulation experiments we conducted to illustrate the effectiveness of our active switching control strategy. The following velocity input was assigned to the leader,

$$v_L(t) = 0.3 \text{ m/s}$$
$$\omega_L(t) = \begin{cases} 0 \text{ rad/s} & \text{if } t \in \{[0,6],(14,20],(28,34]\} \\ \pi/8 \text{ rad/s} & \text{otherwise,} \end{cases}$$

thus corresponding to a piecewise rectilinear-circular trajectory that is particularly suited for testing the proposed control strategy. The formation considered in the simulation experiments consists of two followers. We set $\mathbf{s}(0) = [0.261 \;\; 2.183 \;\; 1.047 \;\; 0.368 \;\; 4.399 \;\; 0.524]^T$ and $\rho_1^{des} = \rho_2^{des} = 0.3$ m., $\psi_1^{des} = 3\pi/4$ and $\psi_2^{des} = 5\pi/4$. The gain matrix of the controller is $\mathbf{K} = 5\,\mathbf{I}_4$, where $\mathbf{I}_4$ denotes the 4×4 identity matrix. The observer $\mathcal{O}$ we used is an EKF initialized with $\hat{\mathbf{s}}(0|-1) = [\frac{3}{2}\rho_1(0) \;\; \psi_1(0) \;\; \beta_1(0) \;\; \frac{3}{2}\rho_2(0) \;\; \psi_2(0) \;\; \beta_2(0)]^T$ corresponding to a 50% perturbation of the unknown distances to the leader and with a covariance matrix $\mathbf{P}(0|-1) = 10^{-2} \cdot \text{diag}\{1, 1.1, 1.1, 1, 1.1, 1.1\}$. The other parameters are $T_c = 10$ ms, $d = 0.1$ m, $\mathbf{Q} = \text{diag}\{3 \cdot 10^{-5}, \varrho, \varrho, 3 \cdot 10^{-5}, \varrho, \varrho\}$ and $\mathbf{R} = \varrho\,\mathbf{I}_4$, where $\varrho = 0.9187 \cdot 10^{-4}$ rad^2. White gaussian noise is added to the measurements.

Fig. 6 shows the robots trajectories in the cases of applying both the *standard* basic control approach of Sect. IV-A (red dotted trajectory) and the *switching active control* of Sect. IV-B-IV-C (blue dashed trajectory). As previously shown, the standard control can not improve the observability along rectilinear tracts, and then the followers are drifting from the nominal trajectory (e.g. $[6, 9]$ s.). In fact, visual data are not changing sensibly so as to improve the localization process against the accumulation of process noises over time.

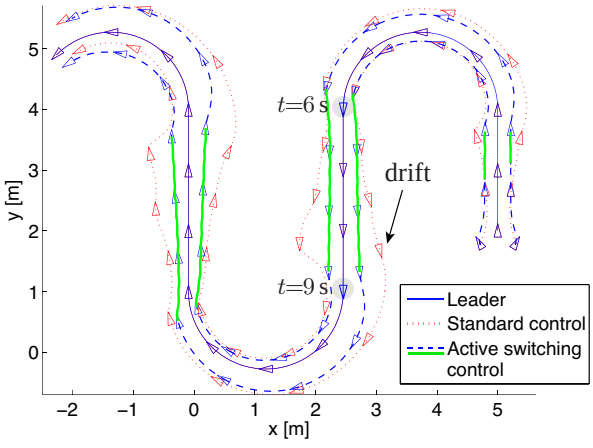

Fig. 6. Simulation results: robot trajectories. While the standard control makes the followers to miss the formation exactly along the rectilinear tracts (e.g. $[6, 9]$ s.), the active switching control maintains the formation and preserves the observability.

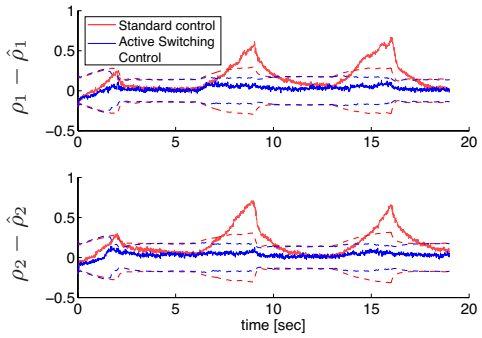

Fig. 7. Simulation results: distance estimation.The active switching control keeps the distance estimation inside the 2σ bounds for all the robot trajectory.

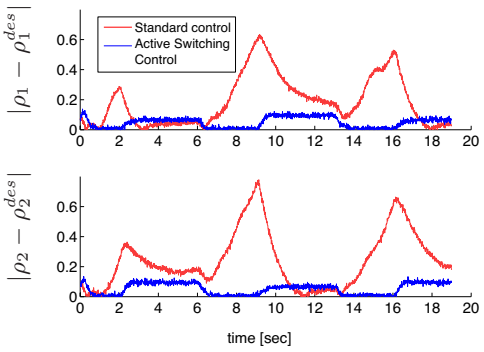

Fig. 8. Simulation results: formation tracking error.

On the other hand the active strategy, automatically activated when the non-observability in detected, successfully preserves both the formation and the system stability (continuous bold green trajectory in Fig. 6). In Fig. 7 we can see the improvement on the localization error $\rho_i - \widehat{\rho}_i$ for each follower: while the error with the standard control leaves the 2σ-bounds exactly along the rectilinear trajectories, in the case of switching control (dark blue line) the distance estimation error *always* remains inside the bounds and stays close to zero.

As expected, since the localization performs better during the whole robot trajectory, also the tracking error $|\rho - \rho^{des}|$ is lower as shown in Fig. 8 especially along rectilinear tracts (e.g. $t = [6, 9]$ s.).

The effects of the active switching control strategy on the $\det(\mathbf{J})$ can be observed in Fig. 9 in which the active control (differently from the standard one) introduces some oscillations so that the observability condition obscillates around zero, but never stabilizes on it, thus avoiding the non observability.

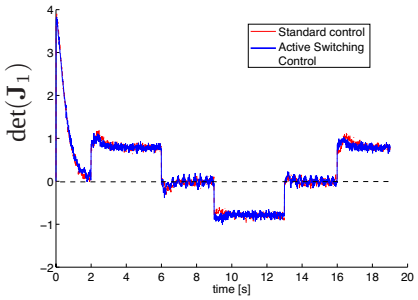

Fig. 9. Simulation results: observability condition for the follower n.1

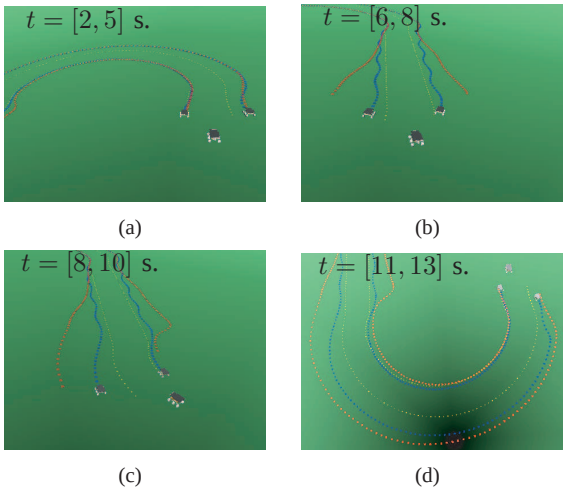

Fig. 10. Snapshots from the video of the simulation experiments.

Fig. 10(a)-(d) shows some snapshots taken from the video of the simulation experiments [1].

In Fig. 11 we show a comparison made over 30 iterations between the tracking errors of active and standard controls, in the case of inter-robot communication delay. As can be seen, the active control (dashed line) outperforms the standard control (continuous line).

VI. Conclusions

Existing strategies for vision-based formation control separate the study of observability from the control design. Observability study is crucial in this context since on-board single camera only provides the view-angle to the other moving robot, but not the distance that must be estimated. The study of observability helps to understand which are the robot motions that influence the system localization performances. In this paper we presented a switching *active* control strategy for formation control. Our control strategy is active, in the sense that integrates both control and recent theoretical results on observability for nonlinear systems in order to guarantee asymptotic achievement of the formation control tasks while also guaranteeing the system observability when all the robots are moving along non-observable paths. In doing this we presented extensive simulation results to show

[1] www.dii.unisi.it/∼gmariottini/ActiveControl-ICRA2009.avi

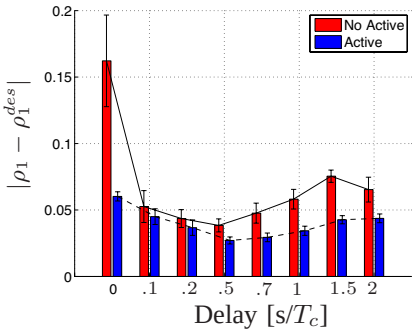

Fig. 11. Tracking error: the active control outperforms the standard control also in the case of increasing communication delay between robots (here as a fraction of the sampling time T_c).

that our strategy improves sensibly the multi-robot system performances (the localization and formation tracking error decreases).

References

[1] J. Cortés, S. Martínez, T. Karatas, and F. Bullo, "Coverage control for mobile sensing networks," *IEEE Trans. Robot. Autom.*, vol. 20, no. 2, pp. 243–255, 2004.

[2] J. Lin, A. Morse, and B. Anderson, "The Multi-Agent Rendezvous Problem," in *Proc. 42nd IEEE Conf. Dec. Contr*, 2003, pp. 1508–1513.

[3] P. Tabuada, G. Pappas, and P. Lima, "Motion Feasibility of Multi-Agent Formations," *IEEE Trans. Robot.*, vol. 21, no. 3, pp. 387–391, 2005.

[4] A. Das, R. Fierro, V. Kumar, J. Ostrowsky, J. Spletzer, and C. Taylor, "A Vision-Based Formation Control Framework," *IEEE Trans. Robot. Autom.*, vol. 18, no. 5, pp. 813–825, 2002.

[5] L. Consolini, F. Morbidi, D. Prattichizzo, and M. Tosques, "Steering hierarchical formations of unicycle robots," in *Proc. 46th IEEE Conf. Decision and Control*, 2007, pp. 1410–1415.

[6] F. Conticelli, A. Bicchi, and A. Balestrino, "Observability and nonlinear observers for mobile robot localization," in *Proc. IFAC Int. Symp. on Robot Control, SyRoCo, 2000*, 2000.

[7] R. Vidal, O. Shakernia, and S. Sastry, "Following the flock: Distributed formation control with omnidirectional vision-based motion segmentation and visual servoing," *IEEE Robot. Autom. Mag.*, vol. 11, no. 4, pp. 14–20, 2004.

[8] A. Das, R. Fierro, V. Kumar, J. Ostrowsky, J. Spletzer, and C. Taylor, "A vision-based formation control framework," *IEEE Trans. on Robot. and Autom.*, vol. 18, no. 5, pp. 813–825, 2002.

[9] A. Isidori, *Nonlinear Control Systems*, 3rd ed. Springer, 1995.

[10] A. Bicchi, D. Prattichizzo, A. Marigo, and A. Balestrino, "On the observability of mobile vehicles localization," in *Proc. IEEE Mediterrean Conf. on Control and Systems*, 1998.

[11] R. Hermann and A. Krener, "Nonlinear controllability and observability," *IEEE Trans. Automat. Contr.*, vol. AC-22, pp. 728–740, 1977.

[12] G. Mariottini, G. Pappas, D. Prattichizzo, and K. Daniilidis, "Vision-based Localization of Leader-Follower Formations," in *Proc. 44th IEEE Conf. Dec. Contr*, 2005, pp. 635–640.

[13] R. Benosman and S. Kang, *Panoramic Vision: Sensors, Theory and Applications*. Springer Verlag, New York, 2001.

[14] A. Blake and M. Isard, *Active Contours*. Springer, 1998.

[15] G. Mariottini, F. Morbidi, D. Prattichizzo, N. V. Valk, N. Michael, G. Pappas, and K. Daniilidis, "Vision-based localization for leader-follower formation control," *IEEE Transactions on Robotics*, 2008, under review.